JOURNAL OF SPACECRAFT AND ROCKETS
Vol. 38, No. 2, March–April 2001

Active Structural-Acoustic Control of a Rocket Fairing Using Proof-Mass Actuators

Steven Griffin*
U.S. Air Force Research Laboratory, Kirtland Air Force Base, New Mexico 87117
Steven A. Lane†
Jackson and Tull Engineering, Albuquerque, New Mexico 87106
and
Colin Hansen‡ and Ben Cazzolato§
University of Adelaide, Adelaide, South Australia 5001, Australia

The feasibility of using proof-mass actuators to control noise transmission actively into a small rocket fairing, given practical constraints on actuator power and mass, is explored. The modal-interaction approach was used to develop a fully coupled structural-acoustic state-space model that relates the out-of-plane structural modal velocities to the spatially varying pressure response in the cavity. The dynamics of the proof-mass actuators were included in the structural-acoustic model. The modal-interaction approach also allowed the decomposition of the acoustic response into radiation modes, which proved essential for determining the optimal locations for sensors and actuators. Numerical simulations using linear quadratic Gaussian controllers with collocated proof-mass actuators and displacement sensors demonstrated approximately 4.2 dB of attenuation over the 300-Hz bandwidth for the given actuator constraints. However, this was only slightly more than the attenuation provided by the passive effects of the proof-mass actuators, which was approximately 3.5 dB.

Nomenclature

$\boldsymbol{A}, \boldsymbol{B}, \boldsymbol{D}$	=	composite stiffness matrices; extensional stiffness, coupling stiffness, and bending stiffness matrix, respectively
$\boldsymbol{A}_2, \boldsymbol{B}_2, \boldsymbol{C}_2$	=	state-space realization of the proof-mass actuator model
$\boldsymbol{A}', \boldsymbol{B}'', \boldsymbol{C}''$	=	state-space realization of the acoustic model
$\boldsymbol{A}, \boldsymbol{H}, \boldsymbol{C}$	=	state-space realization of the structural model
$\boldsymbol{B}$	=	(nondimensionalized) actuator input coupling matrix
$\boldsymbol{B}'''$	=	matrix relating the interior acoustic response to the force loading at the structural nodes
$\boldsymbol{C}_w$	=	vector used to define the velocity difference in the proof-mass actuator model
$\boldsymbol{C}'''$	=	reduced output matrix used to compute the pressure acting at the structural nodes
c_0	=	sound speed in air, m/s
E_p	=	acoustic potential energy, J
$\boldsymbol{F}$	=	diagonal structural-acoustic coupling matrix, kg/m^2/s
$f(t)$	=	force generated by a proof-mass actuator, N
$\boldsymbol{G}$	=	coupling matrix relating interior pressure to structural velocities
$\boldsymbol{H}$	=	matrix relating disturbance inputs at nodes to structural modal response
$i(t)$	=	actuator current, A
J	=	control law performance metric
L	=	coil inductance of a proof-mass actuator, H
m_a, c_a, k_a	=	proof-mass actuator mass, kg; damping, N · s/m; and stiffness, N/m, respectively
m_s, c, k	=	structural system mass, kg; damping, N · s/m; and stiffness, N/m, respectively
$\boldsymbol{p}$	=	column vector giving the pressure at each of the b nodes of the acoustic finite element model, N/m^2
$\mathcal{Q}$	=	state vector weighting penalty
$\boldsymbol{q}$	=	state vector
R	=	coil resistance of a proof-mass actuator, Ω
$\boldsymbol{R}$	=	$c \times c$ nondimensional diagonal matrix that gives the area associated with each structural node as a fraction of the total surface area
$\mathcal{R}$	=	control-effort weighting penalty
$\boldsymbol{r}$	=	state vector of the acoustic system
S	=	surface area of structure, m^2
$\boldsymbol{S}$	=	matrix of eigenvalues, s^{-2}
s	=	Laplace variable, s^{-1}
$\boldsymbol{U}$	=	matrix of eigenvectors, s · kg$^{1/2}$
$\boldsymbol{u}$	=	control inputs, that is, voltage applied to proof-mass actuators, V
$\boldsymbol{V}$	=	$b \times b$ diagonal matrix where the ith diagonal element is the acoustic volume associated with the ith node, m^3
$v_a(t)$	=	voltage applied to a proof-mass actuator, V
$\boldsymbol{v}$	=	vector of pressure inputs, N/m^2
$\boldsymbol{v}_p$	=	$m \times 1$ column vector of modal out-of-plane structural velocities, m/s
$\boldsymbol{w}$	=	structural state vector
$\boldsymbol{x}$	=	vector of structural displacements
$x(t)$	=	system displacement, m
$x_a(t)$	=	actuator displacement, m
$\boldsymbol{y}$	=	vector of structural displacement outputs
$\boldsymbol{y}'$	=	vector of acoustic pressure outputs
$\boldsymbol{z}$	=	state vector of the coupled system
ζ_i	=	modal loss factor of the ith cavity mode (damping ratio)
Λ_i	=	modal volumes of the ith cavity mode, m^3
$\boldsymbol{\Pi}$	=	weighting matrix relating structural velocities to acoustic potential energy, kg
ρ_0	=	air density, kg/m^3
$\boldsymbol{\Phi}$	=	$b \times n$ acoustic mode shape matrix for n unity normalized acoustic modes and for m structural modes
$\boldsymbol{\Phi}'$	=	$c \times n$ acoustic mode shape matrix for the c acoustic nodes that are coincident with structural nodes

Received 23 March 2000; revision received 18 October 2000; accepted for publication 2 November 2000.

*Basic Research Manager, Spacecraft Component Technologies Branch, 3550 Aberdeen Avenue, SE. Member AIAA.
†Research Scientist, Space and Aeronautics Technology Division, 1900 Randolph Road SE, Suite H. Member AIAA.
‡Professor, Department of Mechanical Engineering. Member AIAA.
§Graduate Research Assistant, Department of Mechanical Engineering.

ϕ_i = ith acoustic mode shape
Ψ = $c \times m$ matrix of structural mode shapes orthonormalized with respect to the mass matrix for c structural nodes
ψ = actuator constant, N/A
ω_i = acoustic natural frequency of the ith cavity mode, rad/s

Superscripts

H = Hermitian transpose operator
T = transpose operator

Introduction

An important cause for the failure of many satellites and other launch payloads is the extreme vibrational loading that the payload is subjected to during launch.[1] The predominant source of these vibrations is the explosive reaction of the rocket motors, but aerodynamic buffeting and shocks from stage separations also contribute. The payload may be damaged directly from structural vibrations transmitted through the apparatus attaching the payload to the fairing and from vibration induced by the high-level acoustic environment within the fairing.

As industry and government move toward larger, lightweight fairings, the problem is exacerbated. Furthermore, due to the high costs involved with payload launches, mass and volume are critical quantities that limit the amount of passive treatment that can be added to protect the payload. Therefore, active control technologies are being considered to reduce acoustic and structural vibration loading.[2–6] Active control is more suitable to attenuate noise below 200 Hz, where passive treatments are not practical due to volume constraints.

It is the authors' position that feedforward control strategies do not appear to be practical because it would be difficult, if not impossible, to obtain a coherent measurement of the stochastic disturbance in advance of the control signal or to measure directly the quantity being controlled. The assumption that these measurements are not practical is based on the desire to impose little or no additional interface requirements on the launch vehicle. Therefore, it is not realistic to expect the inclusion of an array of sensors or microphones outside the fairing or throughout the fairing interior as part of a practical active noise control system.

The present work considers the use of feedback control using collocated displacement sensors and proof-mass actuators attached to the fairing. Constraints are placed on the controller that limit the number of actuators and the power available for control to establish a reasonable performance expectation for an actual application. In the following, a fully coupled structural-acoustic model is developed by using a modal-interaction approach[7] and is compared to corresponding finite element models generated by using NASTRAN.[8] Modeling of the proof-mass actuators and coupling their dynamics into the structural-acoustic model is also presented. Sensor and actuator placement to control optimally the dominant structural modes contributing to the dominant acoustic modes is discussed. A model of a realistic, spatially varying acoustic disturbance is developed and used to predict the fairing response at high excitation levels. Design and implementation of dynamic, linear quadratic Gaussian (LQG) control laws that balance control performance and control effort are briefly discussed. Finally, simulations and analysis are presented to indicate reasonable performance expectations for the constrained active control approach using proof-mass actuators and that illustrate important considerations for the fairing noise control problem.

Modeling of the Launch Vehicle Fairing

The modal-interaction approach for the prediction of the interior acoustic response resulting from structural excitation is an alternative method to the fully coupled finite element analysis and is used herein. The modal-interaction approach requires solving both the in-vacuo structural and rigid-wall acoustic cavity problems. These results are then combined to give the solution to the fully coupled problem.[9] This method is computationally less intensive and yields significantly shorter solution times[10] than the fully coupled finite element problem, which requires the fluid-loaded structural mode shapes and flexible boundary acoustic modes. Note that UAI NASTRAN and other commercially available finite element modeling codes also permit a similar analysis, referred to as a modal method, which results in similar gains in computational efficiency. The primary advantage of the modal-interaction method, in the context of structural-acoustic control, is the reformulation of the problem into radiation modes, which will be shown to facilitate greatly efficient placement of sensors and actuators for active control design.

Structural Model

The composite fairing structure was designed to sustain the aerodynamic loads expected during the launch of a small fairing. The design process resulted in the composite stiffness matrices[11] $\boldsymbol{A}$, $\boldsymbol{B}$, and $\boldsymbol{D}$. The next step in modeling the fairing was to determine a grid/skin combination, which provided the required composite stiffness matrices. At the time of this work, these matrices had been determined for the composite fairing, but the final grid/skin combination had not. The geometry had also been determined. In this paper, the modeling of the fairing was done by using the correct $\boldsymbol{A}$, $\boldsymbol{B}$, and $\boldsymbol{D}$ matrices and the correct final geometry, but the grid/skin combination was homogenized, or smeared, into anisotropic shell elements, which only required the geometry and composite stiffness matrices as inputs. The advantage of this method is that it correctly predicts the mode shapes and frequencies of the structural model with fewer elements than a structural model including both the grid and the skin explicitly. The disadvantage is that the local stresses in the skin and the ribs could not be accurately recovered. However, because the local stresses were not required for the structural-acoustic model, this method was entirely sufficient.

Figure 1 presents the geometry of the launch vehicle fairing. The bottom of the fairing was modeled as being rigidly attached to a circular plate, which prevented any motion of the bottom nodes. The rationale behind this selection of boundary conditions was that the majority of the strain energy associated with the structural motion relevant to the acoustic problem occurs in the walls of the fairing and not at the base.[2] Given that the geometry, mechanical properties, and boundary conditions of the fairing had been incorporated into a structural finite element model, the next step was to solve the eigenvalue problem and compute the associated in-vacuo mode shapes and modal (natural) frequencies. The mode shapes and natural frequencies were then combined to form a multiple-input/multiple-output state-space model with pressure or force at the fairing surface as the inputs and structural displacements as outputs. The resulting state-space model is expressed as

$$\dot{\boldsymbol{w}} = \boldsymbol{A}\boldsymbol{w} + \boldsymbol{H}\boldsymbol{v}, \qquad \boldsymbol{y} = \boldsymbol{C}\boldsymbol{w} \tag{1}$$

where $\boldsymbol{w}$ is the $2m \times 1$ structural state vector with m modes, given as

$$\boldsymbol{w} = \begin{bmatrix} \boldsymbol{x} \\ \dot{\boldsymbol{x}} \end{bmatrix} \tag{2}$$

where $\boldsymbol{x}$ and $\dot{\boldsymbol{x}}$ are the $m \times 1$ out-of-plane structural displacement and velocity vectors, respectively. Here, out-of-plane motion is defined to be normal to the tangent plane at any point on the fairing surface. The output $\boldsymbol{y}$ is a vector of structural out-of-plane displacement sensor outputs, and $\boldsymbol{v}$ is a vector of pressure (disturbance) inputs.

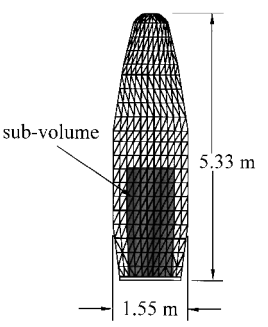

Fig. 1 Geometry of the launch vehicle fairing.

The columns of the $\boldsymbol{H}$ matrix are made up of the out-of-plane vector displacements associated with each mode multiplied by the nodal area associated with the corresponding structural node.

Acoustic Model

The remaining part of the modeling problem is the air cavity enclosed by the fairing structure. If a finite element model is used to obtain the rigid-wall acoustic mode shapes and resonant frequencies, the equation that relates the modal out-of-plane structural velocities to the vector of pressures within the cavity is[12]

$$\boldsymbol{p} = \boldsymbol{\Phi}^T \boldsymbol{F} \boldsymbol{G} \boldsymbol{v}_p \tag{3}$$

The matrix $\boldsymbol{F}$ is an $n \times n$ diagonal matrix whose elements are given by

$$F_{i,j} = \frac{s\rho_0 c_0^2 S}{\Lambda_i \left(s^2 + 2\zeta_i \omega_i s + \omega_i^2\right)} \tag{4}$$

An approximation of Λ_i that is available from the finite element model is

$$\Lambda_i \approx \phi_i^T V \phi_i \tag{5}$$

An approximation for the $n \times m$ coupling matrix $\boldsymbol{G}$ that uses both the acoustic and the structural finite element modeling results is given by

$$\boldsymbol{G} \approx \boldsymbol{\Phi}'^T \boldsymbol{R} \boldsymbol{\Psi} \tag{6}$$

Equation (3) can be converted to a minimal realization multiple-input/multiple-output, state-space model that is relatively insensitive to mathematical precision, as described in Ref. 12. The state-space model of the acoustic system can be expressed as

$$\dot{\boldsymbol{r}} = \boldsymbol{A}'\boldsymbol{r} + \boldsymbol{B}''\boldsymbol{w}, \qquad \boldsymbol{p} = \boldsymbol{C}''\boldsymbol{r} \tag{7}$$

where $\boldsymbol{A}'$ is a $2n \times 2n$ system matrix for n acoustic modes and $\boldsymbol{r}$ is the state vector of the acoustic system model. Because the model realization is not unique, $\boldsymbol{r}$ has no direct physical meaning. The $\boldsymbol{B}''$ matrix has zeros in the first m columns so that the out-of-plane structural velocities $\boldsymbol{v}_p$ are the only inputs to the system in Eq. (7).

Fully Coupled Model

To represent the fully coupled behavior of the system, the structural state-space model must include the acoustic pressure inputs resulting from the radiation state-space model. If $\boldsymbol{C}'''$ is defined as the reduced $\boldsymbol{C}''$ matrix from Eq. (7), which gives only the pressure acting at the structural nodes, the resulting force at the structural nodes is $-\boldsymbol{\Psi} \boldsymbol{A} \boldsymbol{S} \boldsymbol{C}'''\boldsymbol{r}$. Equation (1) can then be expressed as

$$\dot{\boldsymbol{w}} = \boldsymbol{A}\boldsymbol{w} + \boldsymbol{B}'''\boldsymbol{r} + \boldsymbol{H}\boldsymbol{v}, \qquad \boldsymbol{y} = \boldsymbol{C}\boldsymbol{w} \tag{8}$$

where $\boldsymbol{B}''' = -\boldsymbol{\Psi} \boldsymbol{A} \boldsymbol{S} \boldsymbol{C}'''$. The fully coupled model can now be assembled by combining Eqs. (7) and (8) as

$$\dot{z} = \begin{bmatrix} \boldsymbol{A} & \boldsymbol{B}''' \\ \boldsymbol{B}'' & \boldsymbol{A}' \end{bmatrix} z + \begin{bmatrix} \boldsymbol{B} \\ \boldsymbol{0} \end{bmatrix} \boldsymbol{u} + \boldsymbol{H}\boldsymbol{v}$$

$$\boldsymbol{y} = [\boldsymbol{C} \quad \boldsymbol{0}]z, \qquad \boldsymbol{y}' = [\boldsymbol{0} \quad \boldsymbol{C}'']z \tag{9}$$

where

$$z = \begin{bmatrix} \boldsymbol{w} \\ \boldsymbol{r} \end{bmatrix} \tag{10}$$

and $\boldsymbol{B}$ is a matrix that converts the control inputs $\boldsymbol{u}$ into force inputs at the structural nodes.

The fully coupled model given by Eq. (9) was compared to the fully coupled model solved with NASTRAN. The comparison was done by calculating and comparing the responses at points in the cavity due to a random structural disturbance at a location on the fairing for the different modeling approaches. The response at a representative point within the cavity is compared with two corresponding

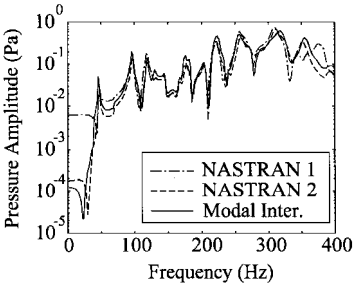

Fig. 2 Comparison of the fully coupled models.

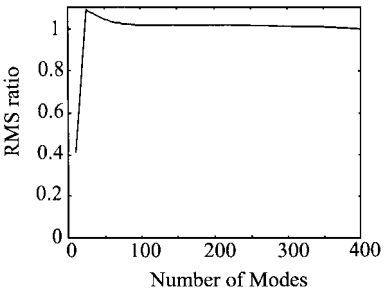

Fig. 3 Ratio of the computed pressure response using modal-interaction models with various numbers of modes to a 400-mode NASTRAN model.

NASTRAN predictions in Fig. 2. The curve labeled NASTRAN 1 solved the fully coupled problem by using the direct method.[8] The curve labeled NASTRAN 2 used the modal method,[8] which post-couples the solutions of the in-vacuo structural and the rigid-wall acoustic problems. The curve labeled Modal Inter. used the modal-interaction model given by Eq. (9). The agreement between all three curves is good in the desired bandwidth, that is, from 50 to 300 Hz.

Another important issue was to determine the number of structural and acoustic modes necessary to have an accurate state-space model. Thus, a series of fully coupled response calculations were made and compared to the response computed using a 400-mode NASTRAN model. The number of structural and acoustic modes used in the modal-interaction model was varied, and in each case the rms of the interior pressure response was calculated for the bandwidth below 300 Hz. Figure 3 presents the ratio of the averaged pressure response using the modal-interaction models to the response computed using a 400-mode NASTRAN model. This shows the influence of the number of modes retained in the model on the spatially averaged interior pressure response. Based on these computations, the retention of 100 modes (50 structural and 50 acoustic) was deemed adequate, which yielded an error in the rms pressure of less than 5% when compared to the 400-mode model.

Controller Development

Sensor and Actuator Placement

The method used to place sensors and actuators was taken from previous work based on the acoustic potential energy within a subvolume of the fairing.[9,10,12] Similar to the free-space radiation problem, the cavity transmission problem can be transformed into radiation modes. For a given subvolume within the fairing (see Fig. 1), the modal expansion for the acoustic potential energy E_p is

$$E_p = \boldsymbol{v}_p^H \boldsymbol{\Pi} \boldsymbol{v}_p \tag{11}$$

The matrix $\boldsymbol{\Pi}$ can be diagonalized by the orthonormal transformation

$$\boldsymbol{\Pi} = \boldsymbol{U}\boldsymbol{S}\boldsymbol{U}^T \tag{12}$$

The real diagonal matrix $\boldsymbol{S}$ contains eigenvalues that can be considered as radiation efficiencies of each radiation mode at a given frequency. The corresponding eigenvectors that make up $\boldsymbol{U}$ give the level of participation of each structural mode in the radiation mode. The solution of Eq. (12) at the frequencies corresponding to the dominant acoustic modes gives a relative measure of the efficiency of each radiation mode for the respective acoustic modes. From this analysis, the radiation modes that dominate the overall acoustic response can be determined. The relative contribution of each structural mode to the dominant radiation modes can be obtained from

the corresponding eigenvector. With focus on controlling the structural modes that most significantly couple to the dominant radiation modes, the acoustic response in the cavity can be reduced. Consequently, locations that couple well with these particular structural modes are optimal positions for structural sensors and actuators. Positions where there is significant overlap of out-of-plane displacement for all of the dominant structural modes can be rank ordered and assigned as necessary depending on the number of sensors and actuators available for control.

Actuator and Sensor Modeling

Because the control actuator that was selected for this work was a proof-mass actuator (PMA), the addition of one PMA will first be described for a single-degree-of-freedom structural model and then generalized to include multiple PMAs for the coupled structural-acoustic fairing model. When a PMA is added to the single-degree-of-freedom spring–mass–damper system shown in Fig. 4, the response of the system can be described by the following second-order differential equations:

$$m_a\ddot{x}_a(t) = -c_a[\dot{x}_a(t) - \dot{x}(t)] - k_a[x_a(t) - x(t)] + f(t)$$

$$m_s\ddot{x}(t) = -cx(t) - kx(t) + c_a[\dot{x}_a(t) - \dot{x}(t)] + k_a[x_a(t) - x(t)] - f(t) \tag{13}$$

The electromechanical dynamics of the PMA can be modeled using a single Kirchhoff's voltage law loop equation:

$$v_a(t) = Ri(t) + L\frac{\mathrm{d}i(t)}{\mathrm{d}t} + \psi[\dot{x}_a(t) - \dot{x}(t)] \tag{14}$$

The force applied by the PMA, $f(t)$, is given as

$$f(t) = \psi i(t) \tag{15}$$

The relative motion between the two masses creates a feedback effect called the back-emf, which affects the force applied to the structure m_s. This system can be modeled with the block diagram formulation presented in Fig. 5. Block 2 of Fig. 5 represents a state-space realization ($\boldsymbol{A}_2$, $\boldsymbol{B}_2$) of the equations of motion presented in Eq. (13), where the state vector $\boldsymbol{q}$ is defined as

$$\boldsymbol{q} = \begin{bmatrix} x \\ x_a \\ \dot{x} \\ \dot{x}_a \end{bmatrix} \tag{16}$$

and the $\boldsymbol{C}_2$ matrix is used to define the desired system outputs. The $\boldsymbol{C}_w$ matrix is defined as

$$\boldsymbol{C}_w = [0 \quad 0 \quad 1 \quad -1] \tag{17}$$

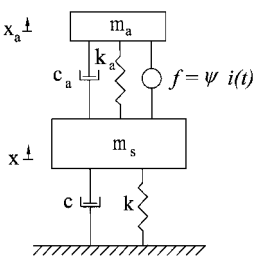

Fig. 4 Proof-mass actuator applied to a single-degree-of-freedom system.

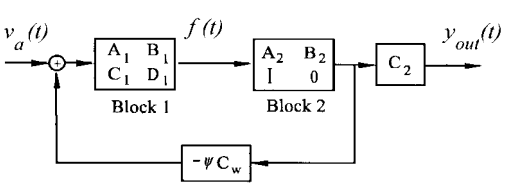

Fig. 5 Block diagram representation of the coupled actuator–structural system.

to provide feedback of the difference in velocities. Solving Eq. (14) for $i(t)$ and substituting into Eq. (15) and then taking the Laplace transform yields the following expression for the force acting on the system:

$$F(s) = [\psi/(R + sL)]\{V_a(s) - \psi s[X_a(s) - X(s)]\} \tag{18}$$

where $s[X_a(s) - X(s)]$ represents the Laplace transform of the difference in velocities. From Eq. (18), it is apparent that block 1 represents a state-space realization of the transfer function

$$\psi/(R + sL)$$

To generalize this approach to the coupled structural-acoustic fairing model, the transfer function in block 1 is converted into a multi-input/multi-output state-space model that reflects the same force-to-voltage relationship for each independent voltage (control) input. The $\boldsymbol{A}_2$ and $\boldsymbol{B}_2$ matrices of the state-space model in block 2 are replaced with the corresponding system matrices from Eq. (9). Substituting the appropriate quantities into the blocks in Fig. 5 yields the fully coupled multi-input/multi-output state-space model using PMAs as control actuators.

Realistic constraints were applied to the control problem to evaluate the feasibility of actually implementing this control approach. The mass of the controller was not to exceed 25% of the total mass of the fairing, which was taken as 63.6 kg in this study. It was assumed that nearly all of the controller mass budget, 15.9 kg, could be allocated to the control actuators. Parameters for the control actuators were taken from an off-the-shelf PMA, the Aura AST-2B-04. It was assumed that the weight of the housing and the heat sink could be reduced due to the relatively short duty cycle required during launch. This resulted in an actual weight of 1.3 kg, which allows 12 actuators. It was also assumed that the maximum rms power limit of 75 W could be relaxed to 100 W. An increased actuator constant of twice the actual value was assumed to allow for improved actuator development. Therefore, the coil resistance and inductance was also doubled. With the use of above-average actuator parameters, the subsequent simulations should provide an upper bound on achievable controller performance for this constrained control approach.

Because 12 actuators were used in control simulations, 12 optimal locations were computed to minimize the acoustic response in the subvolume shown in Fig. 1. Open-loop comparisons were made to determine the effectiveness and optimality of the 12 selected actuator positions. The effectiveness was quantified by the ability of the actuators to generate a response in the fairing subvolume, which indicates coupling and control authority. After the random input signals acting on the 12 actuators positioned at the optimal locations were simulated, the spatially averaged pressure response in the subvolume was computed. This was compared to simulations using the same random inputs with the actuators positioned at arbitrary locations on the structure. Over 300 sets of actuator positions were tested, and, on average, the optimal locations generated 1.35 times the rms pressure response in the subvolume.

Finally, it was assumed that collocated out-of-plane displacement sensors with negligible dynamics could be integrated into the housings of the proof-mass actuators.

Optimal Control Law Design

LQG optimal control laws were designed to minimize a performance index given as

$$J = \int \{z^T \mathcal{Q} z + \boldsymbol{u}^T \mathcal{R} \boldsymbol{u}\}\,\mathrm{d}t \tag{19}$$

where $\mathcal{Q}$ and $\mathcal{R}$ are weighting matrices. Because the state vector includes both the radiation states and the structural states, control effort can be directed at any combination of these quantities. The $\mathcal{Q}$ matrix was assembled so that only the acoustic radiation states were used in the performance index. Defining the $\mathcal{Q}$ matrix as such has been shown in a previous study to be more efficient than a uniform weighting of structural and acoustic states when the objective is to control interior acoustics.[12] The weighting matrix $\mathcal{R}$ was used to balance control effort against the state performance metric to

compute a control law that satisfied the power constraints, that is, less than 100 W per actuator.

Because neither the acoustic states nor the structural states were sensed directly, it was necessary to formulate an optimal estimator, or Kalman–Bucy filter (see Ref. 13). The optimal estimator allowed the reconstruction of the states, including the radiation states, from the structural sensor outputs. The estimated states were then combined with the control law to generate the control signals. Together, the control law and the state estimator formed the dynamic, multi-input/multi-output feedback controllers that were used in subsequent simulations.

Disturbance Modeling

Because one of the objectives of this work was to calculate the power necessary to suppress acoustic transmission under realistic conditions, it was important for the assumed disturbance to be acoustic in nature (as opposed to simply a broadband random input) and of large amplitude. Because of the complexity of the launch problem, it is not possible to get a good representation of the acoustics at launch. However, because a reverberant room test would almost certainly be an intermediate step before a full-scale test of this technology, a disturbance representative of a reverberation test was modeled.

It was assumed that the acoustic field within the cavity dominated the fluid-loading impedance on the structure, which is already included in the fully coupled model. The disturbance can then be modeled as the blocked-surface pressure field and applied to the fully coupled model as an external pressure input. To find the blocked-surface pressure field, additional acoustic fluid elements were generated on the exterior of the fairing structure, which where then modeled as contained within a rigid-wall room of the same geometry of the fairing, but scaled up, as shown in Fig. 6. A constant volume-velocity source was included in one corner of the test room to create an acoustic disturbance. This disturbance model produced a temporally and spatially varying pressure disturbance acting at each node of the fairing structural model.

Because the frequency range of interest was below 300 Hz, it was necessary to make the acoustic elements in the room have characteristic dimensions significantly less than the shortest wavelength of sound, 1.14 m, assuming the sound speed to be 343 m/s. Because it was desired to have relatively diffuse sound in the majority of the frequency range of interest, it was also necessary to make the room dimensions relatively large so that the first room resonance was relatively low. Computational limitations constrained the resulting room dimensions to 17.8×5.17 m. An automeshing routine with an average element characteristic length of 0.25 m generated 119,241 fluid tetrahedron elements in the space between the rigid room walls and the fairing structure. The first room resonance calculated for this geometry was 11.7 Hz. There were 1185 acoustic modes in the frequency range up to 300 Hz, indicating a fairly diffuse sound field.

A random disturbance was injected into the acoustic source for the first 0.5 s and set to zero for the remaining 4.5 s. The resulting time histories of the pressure response at all of the structural node locations (1122) were stored and used as inputs to the coupled structural-acoustic system in the open-loop and closed-loop simulations. The amplitude of the disturbance was scaled so that the spatially averaged rms pressure transmitted to the subvolume was consistent with the interior acoustics for small- or medium-sized launch vehicles (≈140 dB). Figure 7 presents the power spectrum

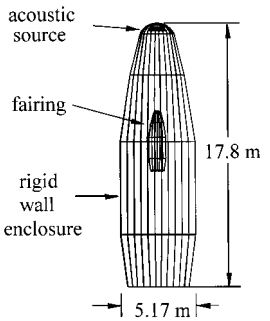

Fig. 6 Geometry of the disturbance model.

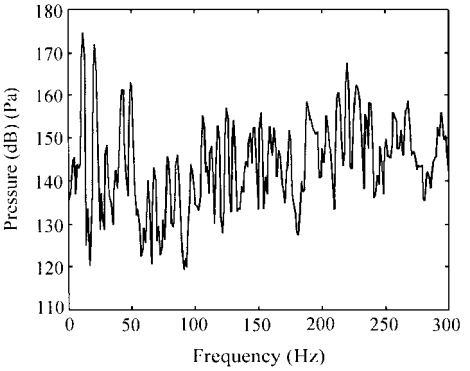

Fig. 7 Power spectrum of the disturbance at a representative point on the fairing.

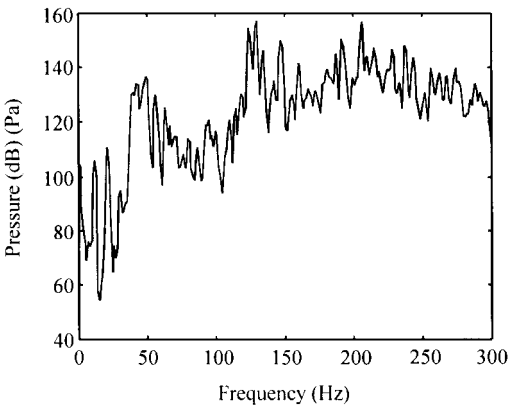

Fig. 8 Power spectrum of the transmitted pressure at a representative point in the subvolume.

of the pressure acting at a representative structural node point on the fairing model in response to the disturbance inputs. Figure 8 shows the power spectrum of the pressure response within the subvolume at a representative point.

Simulations were conducted using MATLAB®[14] to compute the open-loop and closed-loop acoustic response, structural response, and the voltage and current applied to the actuators. From these measurements, the power supplied to the control actuators and the rms pressure reduction achieved across the control bandwidth was computed.

Results

Mounting the proof-mass actuators on the fairing wall changed the structural-acoustic dynamics seen by the disturbance input, which results in some level of transmission loss. To determine the passive effects of the PMAs, a simulation was performed with no control inputs. The response at a representative point within the subvolume to the disturbance is shown in Fig. 9 for the case of no PMAs included in the structural model and with 12 PMAs attached to the fairing structure. An overall spatially averaged rms reduction of 3.54 dB was calculated due to the passive effect of the PMAs. This reduction is attributable to three predominant mechanisms. First, there was the addition of structural damping into the lightly damped structural modes by the heavily damped PMAs. In this case, the damping of the structural modes with no PMAs was assumed to be 1.5%, and the damping of the PMAs was calculated from the manufacturer's data at 10%. Second, the back-emf, which is proportional to the out-of-plane velocity, also contributed damping to the coupled system. Third, the introduction of a spring–mass–damper at a point of large out-of-plane displacement in the dominant structural modes reduced the effectiveness of those modes in transmitting the acoustic disturbance to the fairing interior.[15–17]

The selection of the controller design parameters $\mathcal{Q}$ and $\mathcal{R}$ determines the performance and control effort of the control law. Several choices for the weighting matrix $\mathcal{Q}$ were tested with the best performance resulting from

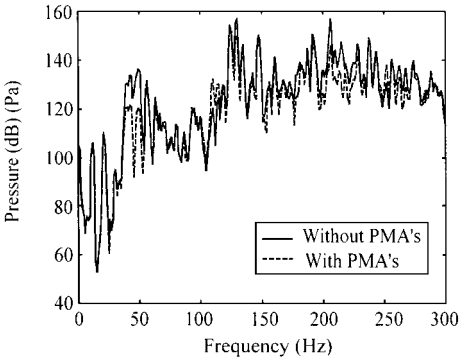

Fig. 9 Comparison of responses at a representative point in the fairing subvolume with and without actuators attached to the fairing (no control input).

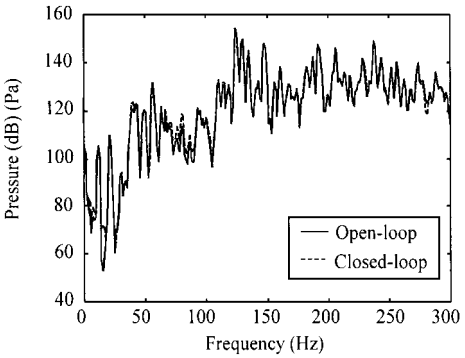

Fig. 10 Comparison of the open-loop and closed-loop responses at a representative point in the fairing subvolume for the power constrained control law.

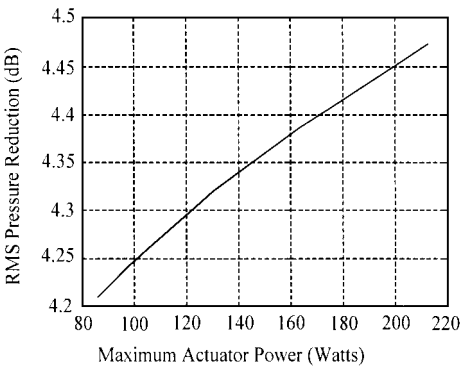

Fig. 11 Plot of the spatially averaged rms pressure reduction attainable in the fairing subvolume as a function of maximum allowed actuator power.

$$\mathcal{Q} = \boldsymbol{C}''^{T}\boldsymbol{C}'' \tag{20}$$

Several simulations were performed while varying the control-effort penalty $\mathcal{R}$ until the maximum rms power delivered to the actuators was close to, without exceeding, 100 W for each actuator. The spatially averaged rms pressure reduction of the closed-loop system using the constrained control law was computed to be 4.2 dB. Figure 10 presents the response spectrum at the same interior point as that used in Fig. 9, but for the case of the closed-loop system. The response is compared to the open-loop (no control input) frequency response. It is apparent that at this representative point, there was very little difference between the open-loop and the closed-loop pressure response. In fact, at some frequencies, the response actually increased. Although the closed-loop system yielded approximately 4.2 dB of overall rms reduction over the bandwidth (300 Hz), the passive effects of simply attaching the PMAs to the fairing structure produced near this level of attenuation.

In Fig. 11, the spatially averaged rms reduction is plotted as a function of the maximum rms power supplied to the actuators. Figure 11 illustrates that, even if the power limit is increased to 200 W per actuator, the estimated reduction only increases to approximately 4.45 dB.

Conclusions

This work presented the essential components needed to explore the physics of the launch vehicle noise problem. The use of a modal-interaction approach provided a multiple-input/multiple-output state-space model that related the out-of-plane structural modal velocity inputs to the spatially varying pressure in the fairing. The modal-interaction approach allowed the decomposition of the acoustic response into radiation modes, which proved to be essential for determining optimal placement of sensors and actuators. The model showed good agreement with finite element models of the fully coupled system. A method for coupling the dynamics of the proof-mass actuators into the model was also presented and provided a means to measure the actuator power requirements.

Reasonable constraints were applied to the active control approach, which limited the mass of the controller and the power available to the controller. Open-loop simulations demonstrated that the passive effects provided by simply coupling the actuators to the structural-acoustic model provided an approximately 3.5-dB reduction in the spatially averaged rms interior response over the 300-Hz bandwidth. Closed-loop simulations using the constrained controller achieved an approximately 4.2-dB reduction in the response for the same bandwidth. The additional weight and complexity required by the active control system hardly seems justified for such a small amount of improvement. Remember that this conclusion is valid only for the specific configuration of this study and cannot be generalized to all approaches for active control of launch vehicles. A much more practical solution to this problem would seem to be to optimize the passive effects of the proof-mass actuators as vibration absorbers or tuned-mass dampers. Because robustness of the controller in the presence of uncertainty between the experimental hardware and the model was not considered, the control simulation results represent the best results that could be hoped for in a hardware implementation. There is room for optimization in the design of the proof-mass actuators for this problem, but even a factor of 2–3 improvement in the force-to-power efficiency of the proof-mass actuator would not significantly increase the reduction in transmission over the passive effects.

Acknowledgments

The authors gratefully acknowledge the support of the U.S. Air Force Office of Scientific Research through both the Windows on Science program and the task "Theoretical and Experimental Studies of Vibroacoustic Systems" under the management of Brian Sanders. The first author would also like to acknowledge the hospitality of the University of Adelaide Mechanical Engineering Department, who hosted him during the initial phase of this research. Finally, the authors would like to thank Donald Leo and Scott Erwin for their insights into the control problem.

References

[1]Timmins, A., and Heuser, R., "A Study of First-Day Space Malfunctions," NASA TN D-6474, Sept. 1971.

[2]Leo, D. J., and Anderson, E. H., "Vibroacoustic Modeling of a Launch Vehicle Payload Fairing for Active Acoustic Control," AIAA Paper 98-2086, April 1998.

[3]Niezrecki, C., and Cudney, H. H., "Preliminary Review of Active Control Technology Applied to the Fairing Acoustic Problem," *AIAA/ASME/AHS Adaptive Structures Forum*, AIAA, Reston, VA, 1996, pp. 101–108.

[4]Denoyer, K., Griffin, S., and Sciulli, D., "Hybrid Structural Acoustic Control of a Sub-Scale Payload Fairing," *SPIE Conference on Smart Structures and Integrated Systems*, edited by M. Regelbrugge, Vol. 3329, Society of Photo-Optical Instrumentation Engineers, Bellingham, WA, 1998, pp. 237–243.

[5]Houston, B., Marcus, M., Bucaro, J., and Williams, E., "Active Control of Payload Fairing Interior Noise Using Physics-Based Control Laws," AIAA Paper 96-1723, May 1996.

[6]Glaese, R., and Miller, D., "Impedance Matching for Structural-Acoustic Control," Ph.D. Dissertation, Dept. of Aeronautics and Astronautics, Massachusetts Inst. of Technology, Cambridge, MA, April 1997.

[7]Fahy, F., *Sound and Structural Vibration*, 1st ed., 4th printing, Academic Press, New York, 1985, pp. 249–255.

[8] *UAI/NASTRAN 20.1 User's Guide*, 6th ed., Vol. 20.1, Universal Analytics, Torrance, CA, 1999, pp. 23.1–23.28.

[9] Cazzolato, B., and Hansen, C., "Active Control of Sound Transmission Using Structural Error Sensing," *Journal of the Acoustical Society of America*, Vol. 104, No. 5, 1998, pp. 2878–2889.

[10] Cazzolato, B., *Sensing Systems for Active Control of Sound Transmission into Cavities*, Ph.D. Dissertation, Dept. of Mechanical Engineering, Univ. of Adelaide, Adelaide, SA, Australia, March 1999.

[11] Agarwal, B. D., and Broutman, L. J., *Analysis and Performance of Fiber Composites*, 1st ed., Wiley, New York, 1980, pp. 145–173.

[12] Griffin, S., Hansen, C., and Cazzolato, B., "Feedback Control of Structurally Radiated Sound into Enclosed Spaces Using Structural Sensing," *Journal of the Acoustical Society of America*, Vol. 106, No. 5, 1999, pp. 2621–2628.

[13] Dorato, P., Abdallah, C., and Cerone, V., *Linear-Quadratic Control*, 1st ed., Prentice–Hall, Englewood Cliffs, NJ, 1995, pp. 99–108.

[14] Matlab 5.3, The Mathworks, Inc., Natick, MA, Jan. 1999.

[15] Fuller, C. R., Silcox, R. J., Metcalf, V. L., and Brown, D. E., "Experiments on Structural Control of Sound Transmitted Through an Elastic Plate," *Proceedings of the 1989 American Control Conference*, Vol. 3, American Autonomous Control Council, Green Valley, AZ, 1989, pp. 2079–2084.

[16] Fuller, C. R., Maillard, J. P., Mercadel, M., and von Flotow, A. H., "Control of Aircraft Interior Noise Using Globally Detuned Vibration Absorbers," *Journal of Sound and Vibration*, Vol. 203, No. 5, 1997, pp. 745–761.

[17] Huang, Y. M., and Fuller, C. R., "Vibration and Noise Control of the Fuselage Via Dynamic Absorbers," *Journal of Vibration and Acoustics*, Vol. 120, No. 2, 1998, pp. 496–502.

M. P. Nemeth
Associate Editor